

# **Lymphatic dysfunction in lupus contributes to cutaneous photosensitivity and lymph node B cell responses**

Mir J. Howlader<sup>1,2,\*</sup>, William G. Ambler<sup>1,3,†,\*</sup>, Madhavi Latha S. Chalasani<sup>1,4,‡</sup>, Aahna Rathod<sup>1</sup>, Ethan S. Seltzer<sup>1,¶</sup>, Ji Hyun Sim<sup>1,4</sup>, Jinyeon Shin<sup>5</sup>, Noa Schwartz<sup>1,6,§</sup>, William D Shipman III<sup>1,7,8,§§</sup>, Dragos C. Dasoveanu<sup>1,9,¶¶</sup>, Camila B. Carballo<sup>10</sup>, Ecem Sevim<sup>6,†</sup>, Salma Siddique<sup>2,6,‡‡</sup>, Yurii Chinenov<sup>11</sup>, Scott A. Rodeo<sup>10,12</sup>, Doruk Erkan<sup>6</sup>, Raghu P. Kataru<sup>5</sup>, Babak Mehrara<sup>5</sup>, Theresa T. Lu<sup>1,2,4,6</sup>

<sup>1</sup>Autoimmunity and Inflammation Program, Hospital for Special Surgery Research Institute; New York, NY, USA

<sup>2</sup>Biochemistry, Structural Biology, Cell Biology, Developmental Biology and Molecular Biology Graduate Program, Weill Cornell Medicine, New York, NY, USA

<sup>3</sup>Pediatric Rheumatology, Department of Medicine, Hospital for Special Surgery; New York, NY, USA

<sup>4</sup>Department of Microbiology and Immunology, Weill Cornell Medicine; New York, NY, USA

<sup>5</sup>Division of Plastic and Reconstructive Surgery, Department of Surgery, Memorial Sloan Kettering Cancer Center; New York, NY, USA

<sup>6</sup>Rheumatology, Department of Medicine, Hospital for Special Surgery; New York, USA

<sup>7</sup>Weill Cornell/Rockefeller/Sloan-Kettering Tri-Institutional MD-PhD Program, New York, NY USA

<sup>8</sup>Immunology and Microbial Pathogenesis Graduate Program, Weill Cornell Medicine, New York, NY, USA

<sup>9</sup>Physiology, Biophysics, and Systems Biology Graduate Program, Weill Cornell Medicine, New York, NY USA

<sup>10</sup>Orthopedic Soft Tissue Research Program, Hospital for Special Surgery Research Institute; New York, NY, USA

<sup>11</sup>David Z. Rosenweig Genomics Research Center, Hospital for Special Surgery Research Institute; New York, NY, USA

<sup>12</sup>Department of Orthopedics, Hospital for Special Surgery; New York, NY, USA

<sup>†</sup>Current address: Systemic Autoimmunity Branch, NIAMS/NIH; Bethesda, Maryland, USA

<sup>‡</sup>Current address: NJ Bio; Princeton, NJ, USA

<sup>¶</sup>Current address: Graduate Program in Bioscience, Rockefeller University; New York, NY, USA

<sup>§</sup>Current address: Department of Medicine (Rheumatology), Albert Einstein College of Medicine/Montefiore Medical Center; Bronx, NY, USA

<sup>§§</sup>Current address: Department of Dermatology, Yale University; New Haven, CT, USA

<sup>¶¶</sup>Current address: Department of Cancer Immunology, Genentech; South San Francisco, CA, USA

<sup>‡‡</sup>Current address: Nemours Hospital for Children, Wilmington, DE, USA

\*Denotes shared first authorship

Corresponding author:

46 Theresa T. Lu  
47 Hospital for Special Surgery  
48 535 East 70<sup>th</sup> Street  
49 New York, NY 10021  
50 Tel: 212-774-2532  
51 Email: [lut@hss.edu](mailto:lut@hss.edu)  
52

53 **Conflict of Interests statement:** The authors have declared that no conflict of interest  
54 exists.

55

## **Abstract**

Patients with systemic lupus erythematosus (SLE) are photosensitive, developing skin inflammation with even ambient ultraviolet radiation (UVR), and this cutaneous photosensitivity can be associated with UVR-induced flares of systemic disease, which can involve increased autoantibodies and further end organ injury. Mechanistic insight into the link between the skin responses and autoimmunity is limited. Signals from skin are transmitted directly to the immune system via lymphatic vessels, and here we show evidence for potentiation of UVR-induced lymphatic flow dysfunction in SLE patients and murine models. Improving lymphatic flow by manual lymphatic drainage (MLD) or with a transgenic model with increased lymphatic vessels reduces both cutaneous inflammation and lymph node B and T cell responses, and long term MLD reduces splenomegaly and titers of a number of autoantibodies. Mechanistically, improved flow restrains B cell responses in part by stimulating a lymph node fibroblastic reticular cell-monocyte axis. Our results point to lymphatic modulation of lymph node stromal function as a link between photosensitive skin responses and autoimmunity and as a therapeutic target in lupus, provide insight into mechanisms by which the skin state regulates draining lymph node function, and suggest the possibility of MLD as an accessible and cost-effective adjunct to add to ongoing medical therapies for lupus and related diseases.

## 77 **Introduction**

78        Photosensitivity, a cutaneous sensitivity to ultraviolet radiation (UVR), affects the  
79 majority of systemic lupus erythematosus (SLE) patients, but, in addition to inflammatory  
80 skin lesions, UVR exposure can trigger systemic disease flares in both patients and  
81 murine models that can include increased autoantibody levels and further end organ  
82 injury (1-5). Currently, medications used for photosensitive skin responses include  
83 topical steroids, topical calcineurin inhibitors, and antimalarials such as  
84 hydroxychloroquine. More importantly, lupus patients are advised to reduce UVR  
85 exposure by avoiding the sun, wearing protective clothing, and wearing sunscreen to  
86 prevent photosensitive skin responses and their sequelae (6-8). Photosensitive skin  
87 inflammation, the accompanying risk of systemic disease flares, and the lifestyle  
88 modifications needed to prevent these all contribute to disrupting patients' quality of life  
89 (9-11). Advances have begun to delineate the mechanisms that contribute to  
90 photosensitivity (12-14). However, the link between UVR-induced skin inflammation and  
91 increased autoantibody titers in these photosensitive patients remains poorly  
92 understood.

93        Skin communicates with lymphoid tissues via lymphatic vessels which transport  
94 cells and interstitial fluid to skin-draining lymph nodes where immune responses occur  
95 and can be regulated. This lymphatic transport serves both to clear fluid and  
96 inflammation from the skin and to deliver antigens, antigen-presenting cells, and  
97 mediators that impact lymph node function (15, 16). Reduced lymphatic flow results in  
98 exacerbated skin inflammation and, over time, can lead to the development of  
99 autoantibodies (17, 18). This latter scenario is not well understood mechanistically but  
100 the combination of skin inflammation and autoimmunity is reminiscent of SLE, and raises



the possibility of lymphatic dysfunction in SLE, which has been described anecdotally (19-22).

Lymphatic flow brings both dendritic cells and lymph fluid to the subcapsular sinus of the draining lymph node, at which point they take divergent paths. Dendritic cells migrating from the skin actively leave the sinus to enter the nodal parenchyma where T and B cells are located (23). Lymph fluid containing soluble molecules, on the other hand, flows into the conduit system (24). The conduits consist of a central collagen core ensheathed by fibroblastic reticular cells (FRCs), and the potential space between the collagen core and the FRCs allows for flow of lymph fluid throughout the lymph node until the lymph leaves the node mainly via efferent lymphatic flow. Comprising the wall of the conduit system, then, FRCs are among the major first sensors of signals flowing from the skin. FRCs, in turn, play critical roles regulating T and B cell responses (25-27), and we recently showed that immunization of healthy mice upregulated FRC-derived CCL2 which promoted CCR2<sup>+</sup> Ly6C<sup>+</sup> monocyte expression of reactive oxygen species (ROS) to limit plasmablast survival (28). Lymphatic input from skin to lymph nodes that alters FRC phenotype, then, could potentially impact lymph node B cell responses.

In this study, we examined for lymphatic dysfunction in both human SLE and murine SLE models and sought to understand the consequences on both skin and lymph node function. We show evidence for potentiation of UVR-induced flow dysfunction in human SLE and in multiple photosensitive SLE models. Improving lymphatic flow by manual lymphatic drainage (MLD) or with a transgenic model with increased lymphatic flow reduced both UVR-induced skin inflammation, draining lymph node B and T cell responses, and MLD over a prolonged period of time reduced splenomegaly and titers of a number of autoantibodies. We further show that improving

lymphatic flow upregulates FRC CCL2, and that depleting monocytes limits the flow-induced reduction in plasmablasts. These results suggest that SLE skin is primed for UVR-induced lymphatic flow dysfunction, and the dysfunction contributes to both cutaneous photosensitive responses and, by modulating a FRC-monocyte axis, lymph node B cell activity in disease. This scenario suggests that improving lymphatic flow and its consequences on the lymph node stromal microenvironment may be therapeutically useful in SLE.

## Results

### *Evidence of dysfunctional dermal lymph flow in SLE patients and mouse models*

We assessed for evidence of lymphatic flow alterations in the skin of SLE patients and SLE mouse models. In human skin, greater lumenal area of lymphatic vessels can be reflective of distention from reduced lymphatic flow (29-31). We examined biopsies that we had previously obtained from the sun-exposed forearm skin of patients with SLE and with persistently positive antiphospholipid antibodies (APL), a condition that can overlap with SLE. These biopsies were taken from sites of livedo reticularis, a lacy pattern of prominent veins on otherwise normal-appearing skin that is not considered to be related to photosensitivity and that affects both SLE and APL patients (32). We compared the samples from SLE patients (some of whom also had APL) to that of APL patients without SLE. SLE skin showed dilated lymphatic vessels when compared to APL-only skin (**Figure 1A-B**). There was no change in the density of lymphatic vessels (**Figure 1C**). While these results are in the context of livedo skin, the differences between SLE and non-SLE patients suggested that there is dysfunctional lymphatic flow in human SLE skin that is exposed to UVR.

We examined lymphatic flow in lupus model mice by assaying for retention in the skin of intradermally injected Evans blue dye (33) after UVR treatment. We focused on ear skin as it has little fur, allowing the skin to be directly exposed to UVR. We used two photosensitive lupus models, the MRL-*Fas*<sup>lpr</sup> (LPR) spontaneous lupus model (34-36) and the imiquimod (IMQ) lupus model that is induced by chronic epicutaneous IMQ application (37). The LPR mice and their MRL-MpJ (MRL) controls were treated with 1000J UVB/m<sup>2</sup>/day of UVR for 4 days prior to Evans blue dye injection in the ear skin (**Figure 1D**). LPR mice showed increased Evans blue dye retention in the ear when compared to MRL mice (**Figure 1E**), suggesting reduced flow out of the ear skin. As

161 expected for the photosensitive LPR mice, there was greater UVR-induced skin swelling  
162 in LPR mice when compared to control MRL mice (**Figure 1F**). The greater Evans blue  
163 dye retention in LPR mice was specific to UVR exposure, as LPR mice showed no  
164 increases in Evans blue dye retention or ear thickness at baseline without UVR (**Figure**  
165 **1G-H**).

166 The UVR-induced lymphatic alterations and ear swelling were accompanied by the  
167 accumulation of inflammatory cells. We had previously shown that inflammatory Ly6C<sup>hi</sup>  
168 monocytes accumulated after one day of UVR in LPR mice (35). After 4 days of UVR,  
169 monocytes numbers accumulated in greater numbers in both MRL and LPR mice treated  
170 with UVR at comparable levels (**Figure 1I**). However, TCR $\alpha\beta$ + CD4 T cells and  
171 TCR $\alpha\beta$ +CD3+CD4-CD8- “double negative” (DN) T cells that are characteristic of LPR  
172 mice (38) both accumulated in greater numbers in LPR mice compared to MRL mice at  
173 this time point (**Figure 1J-K**). Neutrophil, CD8 T cells, and TCR $\gamma\delta$  T cells showed no  
174 changes between LPR and MRL mice (**Supplemental Figure 1A-C**). Together with the  
175 Evans blue dye experiments, these results indicated that lymphatic flow dysfunction  
176 accompanies the increased inflammation in the skin (as indicated by the greater edema  
177 and T cell infiltrate) in UVR-treated LPR mice. These results suggested the possibility  
178 that lymphatic flow dysfunction, by failing to remove fluid and inflammatory mediators  
179 from the skin, was contributing to the increased skin inflammation of the lupus model  
180 mice.

181 We examined the IMQ model (37), inducing this model in B6 mice by applying  
182 IMQ, a TLR7 agonist, to the skin for 4-5 weeks, yielding B6-IMQ mice (**Figure 1L**). IMQ  
183 was applied on the right ear only, and the skin on the rest of the body, including the left  
184 ear, was considered “non-lesional” skin and reflective of systemic disease. We have  
185 shown previously that the “non-lesional” left ear in IMQ mice is similar to non-lesional

skin in human lupus in expressing an interferon signature whereas the right ear has a less robust interferon signature(39). Additionally, the right ear, even without UVR exposure, showed upregulation of apoptotic pathways (**Supplemental Figure 2A**), suggesting that there was tissue damage from repeated local treatment of IMQ. To assess effects of UVR exposure without confounding results from direct IMQ treatment, we focused on the left, non-lesional ear. The left ear showed increased Evans blue dye retention with increased skin swelling upon UVR exposure when compared to vehicle-painted controls (**Figure 1M-N**). Similarly, the footpad of B6-IMQ mice showed increased Evans blue dye retention when compared to B6 mice (**Figure 1O**), suggesting that the dermal lymphatic dysfunction in B6-IMQ mice affected non-lesional skin throughout the body and that the left ear results were not reflective of direct exposure to IMQ that had transferred from the right ear. The right ear also showed increased Evans blue dye retention and increased ear thickness (**Supplemental Figure 2B-C**).

Characterization of the inflammatory infiltrate in B6-IMQ mice showed a higher baseline monocyte number in B6-IMQ compared to B6 mice, and UVR exposure for 1 day showed greater monocyte accumulation in B6-IMQ mice (**Figure 1P**). Monocyte accumulation continued to increase with additional days of UVR exposure, and were equally high in B6-IMQ and B6 ears after 4 days of UVR (**Figure 1P**). In contrast, CD4 T cell number accumulation was limited until after 4 days of UVR, when B6-IMQ showed higher numbers of CD4 T cells than B6 mice (**Figure 1Q**). Neutrophils, TCR $\alpha\beta$  CD8 T cells, and TCR $\gamma\delta$  T cells showed no changes between IMQ and control mice after 4 days of UVR exposure (**Supplemental Figure 1D-F**). Similar to LPR mice, then, B6-IMQ mice showed that UVR-induced skin inflammation after 4 days of treatment included lymphatic dysfunction along with tissue swelling and T cell accumulation. Together, our findings in two distinct SLE models suggested that photosensitive skin is characterized in part by

UVR-induced lymphatic dysfunction, supporting the evidence of lymphatic dysfunction in sun-exposed skin in human SLE.

### ***Improving lymphatic flow reduces photosensitivity of skin in SLE models***

We asked about the contribution of reduced lymphatic flow to cutaneous photosensitive responses in the SLE models by using two different approaches to improve lymphatic flow. One approach was through manual lymphatic drainage (MLD), a technique used by physical therapists to reduce swelling in patients with acquired or congenital lymphedema (40, 41). We administered MLD targeting the left ear once a day during the course of UVR exposure (**Figure 2A-B**). This treatment decreased Evans blue retention in LPR mice relative to handling controls (**Figure 2C and Supplemental Figure 3A**), suggesting that MLD was successful in improving lymphatic flow. MLD also ameliorated UVR-induced skin inflammation, with reductions in ear swelling (**Figure 2D-E**), CD4 T cell numbers and interferon gamma (IFN $\gamma$ ) expression (**Figure 2F-H**), and DN T cell numbers and IFN $\gamma$  expression (**Figure 2I-J**). The proportion of regulatory T cells (Treg) and T helper 17 cells (Th17) within the CD4 T cell population, the proportion of IL-17-expressing DN cells, and the number of CD8 T cells did not change with MLD (**Supplemental Figure 3B-E**). Monocyte and neutrophil numbers also remained unchanged (**Supplemental Figure 3F-G**). These results suggested that improving lymphatic flow with MLD was able to both reduce ear swelling and T cell accumulation and activity in UVR-treated LPR mice.

MLD had similar effects in B6-IMQ mice (**Figure 2K-P**). Evans blue dye retention was reduced (**Figure 2L**), suggesting improved lymphatic flow, and this was accompanied by reduced ear swelling (**Figure 2M**). Both total CD4 T cell numbers and IFN $\gamma$ -expressing Th1 proportion were also decreased with MLD (**Figure 2N-P**). Similar

to LPR mice, MLD had no effect on Treg, Th17, CD8 T cell, monocyte, or neutrophil accumulation (**Supplemental Figure 3H-L**). Our results together suggested that improving lymphatic flow with MLD ameliorated UVR-induced cutaneous inflammation in both the LPR and IMQ SLE models.

Our second approach to improve lymph flow was by using transgenic Flt4Cre<sup>ERT2</sup>PTEN<sup>fl/fl</sup> mice (42). When treated with tamoxifen, these mice have lymphatic endothelial cell (LEC)-specific deletion of PTEN, an antagonist of critical VEGFC/VEGRF3 signaling. This results in expansion of functional lymphatic vessels, improved lymphatic flow from skin, and reduced UVR-induced skin inflammation in healthy (ie non-lupus) mice (42). We confirmed that tamoxifen treatment of Flt4Cre<sup>ERT2</sup>PTEN<sup>fl/fl</sup> mice specifically deleted PTEN from LECs (**Supplemental Figure 4A**). We designated the tamoxifen-treated mice as “LEC<sup>PTEN</sup> mice” and non-tamoxifen-treated mice as “LEC<sup>WT</sup> mice”, and induced the IMQ model in them to generate LEC<sup>PTEN</sup>-IMQ and LEC<sup>WT</sup>-IMQ mice (**Figure 2Q**). Reduced Evans blue dye retention in the left ear of LEC<sup>PTEN</sup>-IMQ mice compared to LEC<sup>WT</sup>-IMQ controls confirmed improved lymphatic drainage (**Figure 2R**), and this was associated with reduced UVR-induced ear swelling (**Figure 2S**), suggesting that improving lymphatic flow reduced the ear swelling. Similar to MLD, the genetic approach to improving lymphatic flow reduced CD4 T cell numbers in LEC<sup>PTEN</sup>-IMQ mice compared to LEC<sup>WT</sup>-IMQ mice (**Figure 2T-U**). Notably, tamoxifen treatment of non-transgenic B6 mice did not reduce Evans blue dye retention or ear swelling (**Figure 2V-W**), suggesting that effects in LEC<sup>PTEN</sup>-IMQ mice were attributable to PTEN deletion rather than to tamoxifen treatment. Treg, CD8 T cell, monocyte, and neutrophil numbers remained unchanged (**Supplemental Figure 3M-P**). The right ear of LEC<sup>PTEN</sup>-IMQ mice also showed reduced Evans blue dye retention and ear swelling when compared to LEC<sup>WT</sup>-IMQ mice and no changes in monocyte and neutrophil

numbers (**Supplemental Figure 4B-E**). As with the left ear, B6-IMQ mice showed no reduction in Evans blue dye retention or ear thickness with tamoxifen (**Supplemental Figure 4F-G**). Consistent with prior reports that improved lymphatic drainage can reduce cutaneous inflammation (33, 42, 43), our results from using both an acute physical approach in two lupus models and a long-term genetic approach showed that improving lymphatic flow from skin reduces cutaneous UVR-induced inflammation in SLE model mice, suggesting that the lymphatic dysfunction contributes to photosensitive skin responses in SLE.

***Improving lymphatic flow reduces draining lymph node B cell responses in SLE models.***

We asked whether lymphatic flow alterations in SLE models contributed to modulating immune activity in downstream lymph nodes. Improving lymphatic flow with MLD over 4 days in LPR mice during UVR exposure did not affect overall lymph node cellularity or overall B cell numbers in draining auricular nodes (**Figure 3A-B**), but did reduce germinal center B cell and plasmablast numbers (**Figure 3C-D**). CD4 T cell numbers were also reduced (**Figure 3E-F**), as was the frequency of TFH cells (**Supplemental Figure 5A**), which could have contributed to reduced germinal center B cell responses. Th1 (**Figure 3G**), Tregs, and Th17 frequencies were unchanged (**Supplemental Figure 5B-C**). CD8 (**Figure 3H**), and DN T cell (**Figure 3I**) numbers were unchanged, as was the expression of IL-17 by DN cells (**Supplemental Figure 5D**). These data suggested that improving lymphatic flow with MLD in LPR mice reduces draining lymph node germinal center and plasmablast responses along with overall CD4 T cell numbers and the proportion of TFH cells.



Similar to LPR mice, MLD in B6-IMQ mice showed no effects on total LN cellularity or on overall B cells (**Fig 3J-K**) but did reduce germinal center B cell, plasmablast, and CD4 T cell numbers (**Fig 3L-O**). Note that the reduction in germinal center (2.2 fold) and plasmablast (2.4 fold) numbers reflects a partial reduction rather than normalization to a non-lupus state, as UVR-treated B6 mice have very few germinal center cells and plasmablasts (1002 $\pm$ 859 and 312 $\pm$ 220 per lymph node, respectively). Unlike in LPR mice, MLD in B6-IMQ mice did not reduce TFH cells (**Supplemental Figure 5E**) but did reduce the TH1 frequency (**Figure 3P**). Tregs and Th17 cell frequencies (**Supplemental Figure 5F-G**) and CD8 T cell numbers (**Figure 3Q**) were unchanged. These data together showed that MLD in LPR and IMQ models reduced B cell responses and CD4 T cell numbers and differentiation, thus suggesting that even a short period of improved lymphatic flow from skin can reduce B and CD4 T cell responses.

In contrast to LPR and B6-IMQ mice treated with MLD, LEC<sup>PTEN</sup>-IMQ mice showed decreases in lymph node cellularity and overall B cells when compared to LEC<sup>WT</sup>-IMQ mice (**Figure 3R-S**). As with LPR and B6-IMQ mice, germinal center B cell, plasmablast, and CD4 T cell numbers were reduced (**Figure 3T-W**). Th1 (**Figure 3X**), TFH, and Treg frequencies (**Supplemental Figure 5H-I**) and CD8 T cell numbers (**Figure 3Y**) were unchanged. These data suggest that improving lymph flow genetically and before induction of lupus disease activity reduced overall lymph node cellularity, and, similar to short term MLD, preferentially reduced B cell and CD4 responses.

### ***Longer duration of improved lymphatic flow reduces systemic disease activity in SLE mice***

While our MLD was targeted to the left ear and draining left auricular lymph node, reduced inflammation at the site of greatest UVR exposure (left ear versus the fur-

covered back, for example) and its draining lymph node could potentially have a systemic effect, as soluble mediators including antigen and inflammatory cytokines can travel from the skin to draining lymph node and then, via efferent flow from the lymph node, out to the systemic circulation to the spleen and end organs (12). Also, reduced B and T cell responses in the draining lymph node would lead to fewer cells and autoantibodies leaving the lymph node to reach the circulation and spleen and other tissues to carry out inflammatory, effector, or memory functions. Furthermore, some inflammatory cells can also leave the skin directly into the blood circulation by reverse transmigration from tissue into blood vessels, as has been shown for neutrophils in UVR-treated skin (44).

We thus asked if improving lymphatic flow in the LEC<sup>PTEN</sup>-IMQ mice or by local MLD can affect parameters of systemic disease activity. We first looked at the splenomegaly that characterizes both the IMQ and LPR models (37, 45). Spleens do not have afferent lymphatics (46) and so splenic changes are considered to reflect systemic changes. LEC<sup>PTEN</sup>-IMQ mice had reduced splenic weight compared to LEC<sup>WT</sup>-IMQ mice (**Figure 4A**), suggesting reduction in systemic disease activity with improved lymphatic flow. To determine if MLD could also affect systemic disease activity, we treated LPR mice with MLD for 4-5 weeks, a duration that would allow indirect splenic changes to occur and for turnover of pre-MLD autoantibodies (47). MLD-treated LPR mice showed reduced splenic weight compared to mice that did not receive MLD, suggesting that longer term MLD can reduce systemic disease (**Figure 4B**). We further measured levels of serum autoantibodies after 4-5 weeks of UVR with and without MLD. While high titer anti-DNA and ribonucleoprotein (RNP) antibodies remained unchanged, antibodies against complement pathway components (C5, C9, Factor B, Factor I, Factor P), histone 2B, and beta2 glycoprotein were reduced (**Fig 4C,D**). Interestingly, LPR mice also

expressed autoantibodies found in dermatomyositis patients (TIF1gamma, Jo1, PL-7, SAE1/SAE2, MDA5, NXP2, mi-2, PM/Scl100) who also demonstrate photosensitivity (48), and some of these (Jo-1, NXP2, PM/Scl100) were also reduced with MLD (**Fig 4C,D**). The reduced splenomegaly and autoantibody levels suggest that longer term MLD can reduce systemic disease activity.

***Improving lymphatic flow increases lymph node FRC CCL2, monocyte ROS generation, and restrains plasmablast responses in a monocyte-dependent manner***

To understand how improving lymphatic flow limits lymph node B cell responses, we considered that FRCs are among the initial sensors of lymph fluid within lymph nodes and asked if improving lymphatic flow could drive an FRC-monocyte axis that we have previously shown to regulate plasmablast accumulation in healthy mice (28). In this axis, stromal CCL2 in the T zone and the medulla induced local CCR2<sup>+</sup> Ly6<sup>hi</sup> monocytes to upregulate ROS expression, which then limited survival of plasmablasts that were colocalized with the CCL2-expressing FRCs and monocytes. Upon MLD of IMQ-treated CCL2-GFP reporter mice, FRCs in the draining auricular lymph nodes showed upregulated GFP, suggestive of upregulated CCL2 expression (**Figure 5A**). By anti-CCL2 staining, an increase in FRC CCL2 was also detectable in LEC<sup>PTEN</sup>-IMQ mice compared with control LEC<sup>WT</sup>-IMQ mice (**Figure 5B**). Additionally, MLD also increased FRC numbers (**Figure 5C**), which likely reflected the increased proliferation rate, as indicated by increased Ki-67 levels (**Figure 5D-E**). This expansion of FRC numbers likely added further to the level of CCL2 sensed by CCR2<sup>+</sup> cells in the lymph node. Together, our results suggested that improving lymphatic flow increased the level of FRC CCL2 in draining lymph nodes.

In association with the stromal CCL2 upregulation, Ly6C<sup>hi</sup> monocyte numbers were unchanged (**Figure 5F**), but monocyte ROS expression was increased (**Figure 5G**). The monocyte ROS increase was specific to this population, as B cells did not show a similar increase (**Figure 5G**). This finding of unchanged monocyte numbers but upregulated ROS expression was consistent with the FRC-monocyte axis in healthy mice (28). Together, these results were consistent with a model whereby improving lymphatic flow increased stromal CCL2 which then increased CCR2+ Ly6C<sup>hi</sup> monocyte expression of ROS to control B cell responses in draining lymph nodes.

To test this model, we took two approaches to ask the extent to which monocytes were required for the reduced B cell responses seen with improved lymphatic flow. We used anti-Gr-1 (28) that depleted both monocytes (**Figure 5H-J**) and neutrophils (**Supplemental Figure 6A**) in B6-IMQ mice during UVR and MLD. This depletion was associated with restoration of germinal center B cell and plasmablast numbers to the higher levels seen in mice without MLD (**Figure 5K-L; compare with Figure 3L-M**), suggesting that MLD-driven reduction in B cell responses was dependent on myeloid cells. To further assess the role of monocytes without depleting neutrophils, we induced the IMQ model in CCR2-DTR mice, injected DT to deplete monocytes (**Figure 5M-O**) but not neutrophils (**Supplemental Figure 6B**), and then treated with UVR and MLD (**Figure 5M**). Germinal center B cell numbers were not altered but plasmablast numbers were restored to the higher levels seen in mice without MLD (**Figure 5P-Q; compare with Figure 3L-M**). The results of the Gr-1 depletion and the CCR2-DTR model together suggested that improved lymphatic flow limits plasmablast accumulation in a monocyte-dependent manner, while the reduction in germinal center B cells is mediated by other mechanisms. All together, our data suggested a model whereby restoring lymphatic flow in UVR-treated SLE mice reduces draining lymph node B cell responses at least in part

by upregulating stromal CCL2 and increasing monocyte ROS to limit plasmablast accumulation.

## **Discussion**

Lymphatic flow is critical for clearing inflammatory mediators from peripheral tissues and communicating with draining lymph nodes, and our results suggested that the link between UVR-induced photosensitive skin responses and increased autoimmunity in SLE is at least in part due to a propensity for SLE skin to develop UVR-induced lymphatic dysfunction. By correcting this dysfunction using either MLD or a transgenic model with increased lymphatic flow, we showed that this lymphatic dysfunction contributed to both upstream cutaneous photosensitive responses and downstream draining lymph node B and T cell responses (**see Figure 6 graphical summary**). While the contribution of lymphatic dysfunction to increasing skin inflammation is consistent with findings in non-lupus models (42, 49), we establish here that lymphatic dysfunction also contributes to B and T cell responses in lymph nodes. Our results suggest that lymphatic dysfunction prevents optimal function of the regulatory FRC-monocyte axis in lymph nodes that normally limits plasmablast responses, and that improving lymphatic function and reducing B cell responses, over the long term, can reduce autoantibody titers. Reduced antibody titers, in turn, has the potential to lead to reduced deposition of immune complexes and limiting inflammation and damage in skin, kidneys, and other end organs. Together, our results suggested that UVR-induced lymphatic flow dysfunction is a contributing factor to lupus pathophysiology and points to lymphatic modulation of lymph node stromal function as a therapeutic target for UVR-induced disease flares.

Our finding that lymphatic flow modulates lymph node stromal phenotype in SLE models underscores the importance of the communication between tissue and lymph nodes and highlights FRC regulation as an outcome of this communication. In this setting, FRCs act as a rheostat that senses and converts peripheral tissue signals into regulators of lymph node activity. We showed that improving flow was connected functionally to the FRC CCL2-monocyte ROS axis that we had previously delineated in the setting of immune responses in non-lupus models. Consistent with the findings in healthy mice, this axis contributed to limiting plasmablast responses and not germinal center responses. Anatomically, CCL2 FRCs are positioned with plasmablasts within the T cell zone and medulla, where they are able to modulate local monocytes, and consequently the plasmablasts (28, 50). FRCs, similar to fibroblasts in the synovium and other tissues (51, 52), are comprised of multiple subsets that have distinct functions related to their anatomic positioning within lymph nodes (25, 26); it will be interesting to further understand how different FRC subsets are modulated phenotypically and functionally by changes in lymphatic flow.

The ways by which lymphatic flow modulates FRC phenotype remains to be determined. FRCs are excellent mechanosensors and respond to environmental alterations to modulate immune function (53-55), and our results may reflect FRC sensing of changes in parameters such as shear stress as lymphatic flow changes. It is also possible that our results reflect FRC sensing of different soluble mediators originating in the skin as lymphatic flow and consequent skin inflammation is modulated (56). For example, with the MLD-induced reduction of T cell interferon gamma expression in skin, there could be reduced levels of interferon that reach the lymph node FRCs, thus altering FRC phenotype. The reduced skin inflammation could also include reduced type I IFN expression in skin, with reduced type I IFN flowing to draining lymph

nodes. Here, it is interesting to note that IFNAR deletion from FRCs has been shown to upregulate FRC CCL2 expression (57), raising the possibility that reduced type I IFN coming from the skin could cause FRC CCL2 upregulation and activate the FRC-monocyte axis to limit B cell responses. Yet another potential way by which improving lymphatic flow can modulation FRC function is that while dendritic cell mobilization from skin to lymph nodes is relatively well preserved even in the face of changes in lymphatic fluid flow (58), dendritic cells can modulate FRC phenotype (59) and skin dendritic cell alterations induced by the reduced skin inflammation upon improving lymphatic flow may potentially alter FRC function upon dendritic cell migration to draining nodes. Further elucidation of how lymphatic manipulation impacts the lymph node stromal compartment will be an important future direction.

The reduced lymphatic flow and relationship to B cell responses in lupus models echoes the findings of Swartz and colleagues who showed in otherwise healthy mice that a dearth of dermal lymphatics leads over time to autoantibodies generation (17). Our data showing that lymphatic function is connected to a lymph node FRC-monocyte axis that we have previously shown in healthy mice (28) to limit B cell responses provides a potential mechanism to explain these findings. This would suggest that the lymphatic regulation of the FRC-monocyte axis is a physiologic mechanism for immune regulation, and that the effects of UVR exposure on autoimmunity in lupus is, in part, a disruption of this physiologic lymphatic-FRC-monocyte axis.

Our study leads to many more questions. It will be interesting to understand the other mechanisms by which lymphatic flow impacted lymph node immune function. For example, the lymphatic-modulated FRC-monocyte axis in lupus model mice contributed to limiting plasma cell responses and not germinal center responses. In LPR mice, reduced TFH numbers by improved lymphatic flow may have contributed to reduced

germinal center responses; how improving lymphatic flow reduced TFH numbers or the T cell interferon gamma expression in both LPR and IMQ models in lymph nodes and the extent to which these changes are the consequence of FRC changes remains to be examined. It will also be interesting to understand the mechanisms by which lupus leads to lymphatic dysfunction. Type I IFN has been shown to inhibit dermal lymphatic fluid transport in the setting of a vaccinia skin infection model (60), suggesting the possibility that the high IFN-I tone in non-lesional human and murine lupus skin (61-64) combined with UVR-induced IFN-I upregulation (65) could be contributing to the lymphatic dysfunction that we observe. The high interferon tone and other features of lupus skin may also contribute to lymphatic flow changes even without UVR exposure that was not captured with our Evans Blue dye assay but that may have immune consequences. Additionally, lymphatic endothelial cells play important roles in regulating the immune cells that enter and migrate within the lymphatics (66-68); the ways in which lymphatic endothelial cell phenotype is altered in lupus skin and the impact on autoimmunity will be interesting to understand going forward.

Our results have clinical implications. Potentially, MLD could be used in addition to current medical therapies to reduce local cutaneous inflammation or, over a larger area over time, to contribute to reducing systemic disease. Examination will be needed to assess the utility of MLD as an accessible and relatively inexpensive adjunct approach to ameliorate disease in SLE.



## **Materials and Methods**

### **Sex as a Biological Variable**

Our study examined male and female animals, and similar findings are reported for both sexes.

### **Study Design**

The purpose of this study was to examine lymphatic function in the skin of photosensitive SLE mouse models and human SLE skin and to understand the contributions of lymphatic function on cutaneous photosensitive and lymph node responses. Laboratory mice were used as subjects for experiments. Human skin sections were also analyzed. Evans blue lymphangiography was used to assess lymphatic flow and flow cytometry was used to identify and quantify cell numbers. For experiments, sample sizes of n=3-21 animals per condition were evaluated in 1 to 11 independent experiments.

### **Human Samples Staining and Imaging**

FFPE sections from skin biopsies of 8 patients with SLE and/or persistently positive APL examined in (32) were used to stain for lymphatic vessels. Patients in the study had active livedo reticularis and staining for lymphatic vessels was done on biopsies taken from the purple areas of the livedo. Five patients had SLE, three of which had concomitant persistent positive APL, and three patients had persistent positive APL without SLE. Two archived samples from healthy donors were also used.

Five micrometer paraffin sections were deparaffinized in xylene and rehydrated in a graded alcohol series. After a final wash with distilled water, specimen slides were

placed in boiling Antigen Unmasking Solution, Tris-Based (Vector Laboratories) for 15 minutes. Slides were briefly washed in water and thereafter in phosphate buffered saline (PBS)-0.025% triton-X-100 prior to blocking non-specific binding sites with PBS-3% bovine serum albumin (BSA) for 30 minutes at room temperature. Double immunostaining was performed with 1:40 dilution in PBS/0.5% BSA of anti-PDPN (D2-40, Biolegend, San Diego, CA) and 1:100 dilution of anti-CD31/PECAM-1 (Novus Biologicals, Centennial, CO) overnight at 4°C. Slides were washed with PBS-0.025% triton-X-100 and endogenous peroxidase was inhibited by incubating slides in 3% H<sub>2</sub>O<sub>2</sub> for 15 minutes in the dark. The sections were then washed in distilled water followed by wash buffer and incubated with alkaline phosphatase-conjugated donkey anti-mouse and horse radish peroxidase-conjugated donkey anti-rabbit secondary antibodies (both Jackson ImmunoResearch, West Grove, PA) at 1:100 dilution (prepared in tris-buffered saline (TBS) with 0.5% BSA) for 1 hour at room temperature. The reaction was revealed with a 3,3'-diaminobenzidine Substrate Kit for peroxidase and fast blue substrate (both Sigma-Aldrich, Burlington, MA) for alkaline phosphatase. At the end of incubation, slides were washed in TBS-0.025% triton-X-100, mounted with Clear-Mount (Electron Microscopy Sciences) and baked at 56°C for 20 minutes. Imaging was performed with Leica Aperio CS2 slide scanner at 40X magnification and ImageJ (NIH) analysis software used to measure the luminal area of PDPN+CD31+ lymphatic vessels. Image analysis was performed blinded to the patient diagnosis.

## **Mice**

Mice between 6-15 weeks of age were used unless otherwise specified. Both male and female mice were used for experiments. All experiments were performed with age and sex matched controls. C57Bl/6, CCL2<sup>-/-</sup> (69), CCL2-GFP (70), MRL<sup>MpJ</sup> (MRL) and MRL-

Fas<sup>lpr</sup> (LPR) mice were originally from Jackson Laboratory (JAX, Bar Harbor, Maine) and bred at our facility. PTEN<sup>fl/fl</sup> CreERT2 (42) were as described. CCR2-DTR (71) mice were bred at our facility.

### **Manual lymphatic drainage**

MLD was adapted to the mouse by a licensed physical therapist (CBC) with experience in MLD. MLD targeting the left ear was performed daily as specified. ProDerma smooth, powder-free latex gloves (Uniseal, Alhambra, CA) were used to minimize friction and cutaneous trauma and all movements were done at a speed of 1-2 seconds per movement. Mice were anesthetized throughout procedure. The first step was the clearing step, and this started with passive motion of the left forelimb, where the mouse was placed in a supine position, held by the paw and clockwise rotations were performed (20 repetitions) to clear the supra-clavicular and axillary area. Subsequently, stationary circular movements with light pressure of the index finger were applied on the left submandibular area followed by the auricular area (20 reps each). The mouse was then placed in the right lateral decubitus position to proceed with the reabsorption step which was performed in a specific sequence: 1. The left ear was held gently with a pincer grip (thumb and index finger) and light sweeping movements with the index finger were done on the ventral surface of the ear from distal to proximal (50 reps); 2. Placed in a prone position, the ear was gently held with a pincer grip and sweeping movements were done from distal to proximal on the dorsum of the base of the ear (where the large collecting lymphatic vessels are and can be visualized by Evan's blue lymphangiography) (200 reps); 3. Placed back to the right lateral decubitus position, sweeping movements at the base of the ear toward the auricular lymph node were performed (20 reps); 4. Finally placed in supine position again, the same clockwise

rotations of the left forelimb was performed (20 reps). Handling controls were anesthetized in the same manner as for MLD, and the mouse was placed prone and left ear was held with a pincer grip similarly to MLD for 5 minutes.

#### **Mouse treatments**

For UVR treatments, mice were exposed to 1000 - 1500 J UVB/m<sup>2</sup>/day for four consecutive days using a bank of four FS40T12 sunlamps, as previously described (35).

For long term treatment, mice were exposed to UVR for four consecutive days the first week and then for 3 consecutive days/week in the following weeks. To measure ear swelling after UVR exposure, a caliper (Mitutoyo, Industry, CA) was used. Each ear was measured in the anterior half of the ear three times and the average was taken.

For the IMQ-induced lupus mouse model, mice were painted on the dorsal and ventral sides of the right ear with 5% imiquimod cream (Taro Pharmaceutical) 3x/week for 4-5 weeks (~50 mg/mouse total cumulative dose) (37).

For mice receiving tamoxifen, tamoxifen (Sigma-Aldrich) in corn oil was injected intraperitoneally (IP) at a dose of 300mg/kg/day every other day for three doses.

For monocyte depletion studies in the B6-IMQ mice, anti-Gr1 (RB6-8C5) or isotype control IgG (LTF-2) (both BioXCell, Lebanon, NH) were injected IP at a dose of 250µg in 200µl PBS on indicated days. To deplete monocytes in the CCR2-DTR mice, diphtheria toxin (Enzo Life Sciences, Farmingdale, NY) was injected IP at a dose of 250ng in 200 ul PBS.

#### **Evans blue lymphatic function assay**

Evans blue retention assay was performed as previously described (72). Mouse ears were injected intradermally at the tip using a Hamilton syringe (#1701, 10 ul syringe) with a 30-gauge needle. 1µl of 2% Evans blue (Sigma-Aldrich) was injected and mice were euthanized 22-24 hours later. The harvested ear was placed in 300µl formamide at 58°C overnight to extract Evans blue, which was quantified by absorbance with a Multiskan Ascent plate reader (Titertek, Pforzheim, Germany) at 620nm using a titration curve.

### **ROS Staining**

Intracellular ROS was measured using 5-(and6)chloromethyl-2',7'-dichlorodihydrofluorescein diacetate, acetyl ester (CM-H<sub>2</sub>DCFDA, Thermo Fisher Scientific), as in (28). The dye was reconstituted at 5 mmol/L in DMSO and stored at -20°C. Cells were prepared in RPMI and stained with 1/500 dilution of the stock in PBS for 30 minutes at 37°C prior to flow cytometric analysis.

### **Flow cytometry staining and quantification**

For flow cytometric staining of skin, single cell suspensions were generated as previously described (73). In brief, ears were finely minced, digested in type II collagenase (616 U/mL; Worthington Biochemical Corporation, Lakewood, NY), dispase (2.42 U/mL; Life Technologies, Carlsbad, CA), and DNase1 (80 µg/mL; Sigma-Aldrich), incubated at 37°C while shaking at 100 rpm, triturated with glass pipettes, and filtered. For staining of lymph node cells, hematopoietic cells from lymph nodes were obtained by mashing the lymph nodes and extruding the cells through a 70µm strainer. Stromal cells were obtained as previously described (74); lymph nodes were minced, digested with type II collagenase (616 U/mL) and DNase1 (40µg/mL) at 37°C while shaking at 50 rpm, triturated with glass pipettes, and filtered.

605

606 To count cells, the single cell suspension from the whole lymph node or ear was washed  
607 and resuspended in 300 ul of buffer. Ten ul was taken to be counted on the Multisizer 4e  
608 Coulter Counter (Beckman Coulter) and this count was used to calculate total number of  
609 cells per lymph node. One to two million cells per sample were stained, and most of the  
610 sample was run on the flow cytometer. To obtain absolute number of a particular  
611 population of cells per ear or lymph node, the frequency of these cells (of the total) in the  
612 facs analysis was multiplied by the total number of cells per tissue (as calculated by the  
613 Counter Counter data).

614

615 For flow cytometry analysis, gating of specific populations was performed after excluding  
616 debris, doublets, and dead cells using 4',6-diamidino-2-phenylindole dihydrochloride  
617 (DAPI, Invitrogen) for non-fixed cells. Antibodies are from Biolegend unless otherwise  
618 specified. Samples were treated with anti-mouse CD16/32 (Fc block, clone 93) prior to  
619 staining with additional antibodies. Gating strategies and antibodies used-- B cells:  
620 CD45+(30-F11) B220+(RA3-6132); monocytes: CD45+, B220-, CD3-(145-2C11),  
621 CD11b+(M1/70), Ly6C<sup>hi</sup>(HK1.4), Ly6G-(1A8); neutrophils: CD45+, CD11b+, Ly6C<sup>med</sup>,  
622 Ly6G+; germinal center B cells: CD3-, B220+, GL7+(GL7), PNA+(Vector Laboratories);  
623 plasmablasts: CD3-, B220med-lo, CD138+(281-2). In digested tissues, plasmablasts  
624 were identified by either intracellular IgG (IgG1-A85-1, IgG2a/b-R2-40, IgG3-R40-82, all  
625 BD Biosciences) or intracellular Ig kappa+(187.1) (Southern Biotech) using BD  
626 Cytofix/Cytoperm kit (BD Biosciences) in lieu of CD138. Plasmablasts were confirmed by  
627 Ki67(16A8) staining. Lymphatic endothelial cells: CD45-, CD31+ (390), PDPN+ (8.1.1);  
628 blood endothelial cells: CD45-CD31-, PDPN-; fibroblastic reticular cells: CD45-, CD31-,  
629 PDPN+. CD4 T cells: CD45+CD4+TCRab+ (H57-597); regulatory T cells: TCRab+,

CD4+, CD25+ (PC61), intracellular Foxp3+ (FJK-16s); follicular helper T cells: TCRab+, CD4+, CXCR5+ (L138D7), PD1+ (29F.1A12); Th1 cells: TCRab+, CD4+, Foxp3-, CXCR5 -, intracellular IFN $\gamma$ + (XMG1.2, eBioscience); Th17 cells: TCRab+, CD4+, Foxp3-, CXCR5-, intracellular IL17+ (TC11-18H10, BD Biosciences). The intracellular stains for CD4+ T cell subset was done after fixing cells with the eBioscience™ Intracellular Fixation & Permeabilization Buffer Set (Cat: 88-8824-00). For Th1 and Th17 cells, staining was done after cells were stimulated with Cell Activation Cocktail with Brefeldin A (Biolegend, Cat no. 423304) in 37C incubator for 4 hours. CCL2 was identified by either using CCL2-GFP reporter mice or by staining. Staining for CCL2 was performed using CCL2-FITC (2H5, Invitrogen) and signal was amplified by staining with anti-FITC-biotin (1F8-1E4, Jackson ImmunoResearch) and subsequently streptavidin-FITC (Invitrogen). A negative control for GFP signal was done by using non-transgenic mice in CCL2-GFP mice experiments. CCL2<sup>-/-</sup> mice were used as negative control for staining experiments.

For a detailed list of all used antibodies, refer to **Supplemental Table 1**.

For flow cytometry analysis, cells were analyzed using a FACSCanto or FACSSymphony (BD Biosciences) and FlowJo Software (Tree Star).

#### **Cell Sorting:**

For qPCR of skin cell populations, cells from ear skin were pooled and then sorted using a BD Influx (BD Biosciences). LECs were selected as DAPI-CD45-PDPN+CD31+ cells. BECs were selected as DAPI-CD45-PDPN-CD31+ cells. Fibroblasts were selected as DAPI-CD45-PDPN+CD31- cells. Macrophages were selected as DAPI-CD45+CD11b+F4/80+ cells.

655

## 656 **RNA Extraction**

657 RNA was extracted from sorted cells using an RNAEasy Plus Kit (Qiagen, Germantown,  
658 MD) and quality confirmed on a BioAnalyzer 2100 (Agilent Technologies, Santa Clara,  
659 CA).

660

## 661 **Real time PCR**

662 cDNA was synthesized (iScript kit, Bio-Rad, Hercules, CA) from extracted RNA and real-  
663 time PCR (iQ SYBR-Green Supermix kit, Bio-Rad)) was performed using primers for  
664 PTEN (Mm\_Pten\_1\_SG QuantiTect Primer Assay, Qiagen) and GAPDH (R:  
665 TTGAAGTCGCAGGAGACAACCT, F: ATGTGTCCGTCGTGGATCTGA).

666

## 667 **Autoantigen Microarray:**

668 Blood was collected from mice, left at room temperature for 1 hour, and then centrifuged  
669 at 3000rpm for 3 minutes. The supernatant containing the serum was then collected and  
670 frozen in -80C until ready to be shipped for autoantigen microarray profiling at the  
671 Genomics and Microarray Core Facility, UT Southwestern Medical Center.

672

## 673 **Statistics**

674 For figures showing normalized values, each individual replicate experiment was  
675 normalized for that experiment. For experiments that contained more than one control  
676 sample, the mean was obtained for the control samples, and the individual control and  
677 experimental samples were divided by this mean value to normalize to the control mean.  
678 The Shapiro-Wilk test was used to test for normality. Unpaired t test was used for normal  
679 data and Mann-Whitney U test was used otherwise.



## **Study Approval**

All animal experiments and research plans were approved by the Institutional Animal Care and Use Committee at Weill Cornell Medicine (New York, NY). Ethical approval for human studies was obtained from Hospital for Special Surgery Institutional Review Board (IRB) (IRB number: 2015-256), where participants had signed written informed consents for both the initial study and for the subsequent study of skin biopsies.

## **Data Availability**

The murine RNAseq data has been previously published and is publicly available in GEO (GSE255519 for IMQ mice) (39).

691 **Author Contributions**

692 WGA, NS, and TTL conceived the study; MJH, WGA, MLC, AR, ESS, JHS, JS, NS, WDS,  
693 DCD, CBC, RPK, YC designed and performed the experiments and analyzed the data;  
694 ES, DE, SS, RPK, and BM provided key reagents and intellectual input. CBC and SAR  
695 designed experiments and provided intellectual input. TTL designed, supervised, and  
696 interpreted experiments. MJH, WGA, and TTL wrote the manuscript; all authors  
697 contributed to critical reading and editing.

## **Acknowledgments**

The authors thank the Lu Lab for critical reading of the manuscript. This work was supported by R01AI079178-121S1 (MJH), NIH T32AR071302-01 to the Hospital for Special Surgery Research Institute Rheumatology Training Program (NS and WDS), NIH MSTP T32GM007739 to the Weill Cornell/Rockefeller/Sloan-Kettering Tri-Institutional MD-PhD Program (WDS), Emerson Collective Cancer Research Fund 691032 (RPK), NIH R01AI079178 (TTL), R01AR084694 (TTL), R21 AR081493 (TTL), DOD W81XWH-22-1-0627(TTL), Lupus Research Alliance (TTL), the St. Giles Foundation (TTL); and NIH Office of the Director grant S10OD019986 to Hospital for Special Surgery. Schematics in figures were created in BioRender. Lu, T. (2025) <https://BioRender.com/8ksl0q5>

## 711 References

- 712 1. Tsokos GC, Lo MS, Costa Reis P, and Sullivan KE. New insights into the  
713 immunopathogenesis of systemic lupus erythematosus. *Nat Rev Rheumatol*.  
714 2016;12(12):716-30.
- 715 2. Stannard JN, and Kahlenberg JM. Cutaneous lupus erythematosus: updates on  
716 pathogenesis and associations with systemic lupus. *Curr Opin Rheumatol*.  
717 2016;28(5):453-9.
- 718 3. Schmidt E, Tony HP, Bröcker EB, and Kneitz C. Sun-induced life-threatening lupus  
719 nephritis. *Annals of the New York Academy of Sciences*. 2007;1108:35-40.
- 720 4. Foering K, Chang AY, Piette EW, Cucchiara A, Okawa J, and Werth VP. Characterization  
721 of clinical photosensitivity in cutaneous lupus erythematosus. *Journal of the American*  
722 *Academy of Dermatology*. 2013;69(2):205-13.
- 723 5. Ansel JC, Mountz J, Steinberg AD, DeFabo E, and Green I. Effects of UV radiation on  
724 autoimmune strains of mice: increased mortality and accelerated autoimmunity in BXSB  
725 male mice. *J Invest Dermatol*. 1985;85(3):181-6.
- 726 6. Ahluwalia J, and Marsch A. Photosensitivity and photoprotection in patients with lupus  
727 erythematosus. *Lupus*. 2019;28(6):697-702.
- 728 7. Kuhn A, Gensch K, Haust M, Meuth AM, Boyer F, Dupuy P, et al. Photoprotective effects  
729 of a broad-spectrum sunscreen in ultraviolet-induced cutaneous lupus erythematosus: a  
730 randomized, vehicle-controlled, double-blind study. *J Am Acad Dermatol*. 2011;64(1):37-  
731 48.
- 732 8. Vilá LM, Mayor AM, Valentín AH, Rodríguez SI, Reyes ML, Acosta E, et al. Association of  
733 sunlight exposure and photoprotection measures with clinical outcome in systemic  
734 lupus erythematosus. *P R Health Sci J*. 1999;18(2):89-94.
- 735 9. Mikita N, Ikeda T, Ishiguro M, and Furukawa F. Recent advances in cytokines in  
736 cutaneous and systemic lupus erythematosus. *J Dermatol*. 2011;38(9):839-49.
- 737 10. Ogunsanya ME, Kalb SJ, Kabaria A, and Chen S. A systematic review of patient-reported  
738 outcomes in patients with cutaneous lupus erythematosus. *Br J Dermatol*.  
739 2017;176(1):52-61.
- 740 11. Tebbe B, and Orfanos CE. Epidemiology and socioeconomic impact of skin disease in  
741 lupus erythematosus. *Lupus*. 1997;6(2):96-104.
- 742 12. Sim JH, Ambler WG, Sollohub IF, Howlader MJ, Li TM, Lee HJ, et al. Immune Cell–Stromal  
743 Circuitry in Lupus Photosensitivity. *The Journal of Immunology*. 2021;206(2):302-9.
- 744 13. Kahlenberg JM. Rethinking the Pathogenesis of Cutaneous Lupus. *J Invest Dermatol*.  
745 2021;141(1):32-5.
- 746 14. Patel J, Borucki R, and Werth VP. An Update on the Pathogenesis of Cutaneous Lupus  
747 Erythematosus and Its Role in Clinical Practice. *Curr Rheumatol Rep*. 2020;22(10):69.
- 748 15. Oliver G, Kipnis J, Randolph GJ, and Harvey NL. The Lymphatic Vasculature in the 21(st)  
749 Century: Novel Functional Roles in Homeostasis and Disease. *Cell*. 2020;182(2):270-96.
- 750 16. Fonseca DM, Hand TW, Han SJ, Gerner MY, Glatman Zaretsky A, Byrd AL, et al.  
751 Microbiota-Dependent Sequelae of Acute Infection Compromise Tissue-Specific  
752 Immunity. *Cell*. 2015;163(2):354-66.
- 753 17. Thomas SN, Rutkowski JM, Pasquier M, Kuan EL, Alitalo K, Randolph GJ, et al. Impaired  
754 Humoral Immunity and Tolerance in K14-VEGFR-3-Ig Mice That Lack Dermal Lymphatic  
755 Drainage. *The Journal of Immunology*. 2012;189(5):2181-90.

- 756 18. Kajiya K, and Detmar M. An Important Role of Lymphatic Vessels in the Control of UVB-  
757 Induced Edema Formation and Inflammation. *J Invest Dermatol.* 2006;126(4):920-2.
- 758 19. Rajasekhar L, Habibi S, Sudhakar P, and Gumdal N. Lymphatic obstruction as a cause of  
759 extremity edema in systemic lupus erythematosus. *Clin Rheumatol.* 2013;32 Suppl  
760 1:S11-3.
- 761 20. Daniel A, Bagnato G, Vital E, and Del Galdo F. Chylous ascites in a patient with an  
762 overlap syndrome: a surprising response to rituximab. *BMJ case reports.* 2017;2017.
- 763 21. Dalvi SR, Yildirim R, Santoriello D, and Belmont HM. Pseudo-pseudo Meigs' syndrome in  
764 a patient with systemic lupus erythematosus. *Lupus.* 2012;21(13):1463-6.
- 765 22. Lee CK, Han JM, Lee KN, Lee EY, Shin JH, Cho YS, et al. Concurrent occurrence of  
766 chylothorax, chylous ascites, and protein-losing enteropathy in systemic lupus  
767 erythematosus. *J Rheumatol.* 2002;29(6):1330-3.
- 768 23. Ulvmar MH, Werth K, Braun A, Kelay P, Hub E, Eller K, et al. The atypical chemokine  
769 receptor CCRL1 shapes functional CCL21 gradients in lymph nodes. *Nat Immunol.*  
770 2014;15(7):623-30.
- 771 24. Gretz JE, Norbury CC, Anderson AO, Proudfoot AE, and Shaw S. Lymph-borne  
772 chemokines and other low molecular weight molecules reach high endothelial venules  
773 via specialized conduits while a functional barrier limits access to the lymphocyte  
774 microenvironments in lymph node cortex. *J Exp Med.* 2000;192(10):1425-40.
- 775 25. Li L, Wu J, Abdi R, Jewell CM, and Bromberg JS. Lymph node fibroblastic reticular cells  
776 steer immune responses. *Trends Immunol.* 2021;42(8):723-34.
- 777 26. Pikor NB, Cheng H-W, Onder L, and Ludewig B. Development and Immunological  
778 Function of Lymph Node Stromal Cells. *The Journal of Immunology.* 2021;206(2):257-63.
- 779 27. Krishnamurty AT, and Turley SJ. Lymph node stromal cells: cartographers of the immune  
780 system. *Nat Immunol.* 2020;21(4):369-80.
- 781 28. Dasoveanu DC, Park HJ, Ly CL, Shipman WD, Chyou S, Kumar V, et al. Lymph node  
782 stromal CCL2 limits antibody responses. *Sci Immunol.* 2020;5(45).
- 783 29. Yazici Y, Erkan D, Levine DM, Parker TS, and Lockshin MD. Protein-losing enteropathy in  
784 systemic lupus erythematosus: report of a severe, persistent case and review of  
785 pathophysiology. *Lupus.* 2002;11(2):119-23.
- 786 30. von der Weid PY, Rehal S, and Ferraz JG. Role of the lymphatic system in the  
787 pathogenesis of Crohn's disease. *Curr Opin Gastroenterol.* 2011;27(4):335-41.
- 788 31. Rossi A, Sozio F, Sestini P, Renzoni EA, Khan K, Denton CP, et al. Lymphatic and blood  
789 vessels in scleroderma skin, a morphometric analysis. *Human Pathology.*  
790 2010;41(3):366-74.
- 791 32. Sevim E, Siddique S, Chalasani MLS, Chyou S, Shipman W, O'Shea O, et al. Mammalian  
792 Target of Rapamycin Pathway Assessment in Antiphospholipid Antibody Positive  
793 Patients with Livedo. *J Rheumatol.* 2022.
- 794 33. Huggenberger R, Siddiqui SS, Brander D, Ullmann S, Zimmermann K, Antsiferova M, et  
795 al. An important role of lymphatic vessel activation in limiting acute inflammation.  
796 *Blood.* 2011;117(17):4667-78.
- 797 34. Furukawa F. Photosensitivity in cutaneous lupus erythematosus: lessons from mice and  
798 men. *J Dermatol Sci.* 2003;33(2):81-9.
- 799 35. Shipman WD, Chyou S, Ramanathan A, Izmirly PM, Sharma S, Pannellini T, et al. A  
800 protective Langerhans cell–keratinocyte axis that is dysfunctional in photosensitivity.  
801 *Science Translational Medicine.* 2018;10(454):eaap9527.

- 802 36. Menke J, Hsu MY, Byrne KT, Lucas JA, Rabacal WA, Croker BP, et al. Sunlight Triggers  
803 Cutaneous Lupus through a CSF-1-Dependent Mechanism in MRL-Fas<sup>lpr</sup> Mice. *J*  
804 *Immunol.* 2008;181(10):7367-79.
- 805 37. Yokogawa M, Takaishi M, Nakajima K, Kamijima R, Fujimoto C, Kataoka S, et al.  
806 Epicutaneous application of toll-like receptor 7 agonists leads to systemic autoimmunity  
807 in wild-type mice: a new model of systemic Lupus erythematosus. *Arthritis Rheumatol.*  
808 2014;66(3):694-706.
- 809 38. Mizui M, Koga T, Lieberman LA, Beltran J, Yoshida N, Johnson MC, et al. IL-2 protects  
810 lupus-prone mice from multiple end-organ damage by limiting CD4-CD8- IL-17-  
811 producing T cells. *J Immunol.* 2014;193(5):2168-77.
- 812 39. Li TM, Zylina V, Seltzer ES, Dacic M, Chinenov Y, Daamen AR, et al. The interferon-rich  
813 skin environment regulates Langerhans cell ADAM17 to promote photosensitivity in  
814 lupus. *Elife.* 2024;13.
- 815 40. Lurie F, Malgor RD, Carman T, Dean SM, lafrati MD, Khilnani NM, et al. The American  
816 Venous Forum, American Vein and Lymphatic Society and the Society for Vascular  
817 Medicine expert opinion consensus on lymphedema diagnosis and treatment.  
818 *Phlebology.* 2022;37(4):252-66.
- 819 41. Lasinski BB, McKillip Thrift K, Squire D, Austin MK, Smith KM, Wanchai A, et al. A  
820 systematic review of the evidence for complete decongestive therapy in the treatment  
821 of lymphedema from 2004 to 2011. *Pm r.* 2012;4(8):580-601.
- 822 42. Kataru RP, Baik JE, Park HJ, Ly CL, Shin J, Schwartz N, et al. Lymphatic-specific  
823 intracellular modulation of receptor tyrosine kinase signaling improves lymphatic  
824 growth and function. *Sci Signal.* 2021;14(695):eabc0836.
- 825 43. Schwager S, Renner S, Hemmerle T, Karaman S, Proulx ST, Fetz R, et al. Antibody-  
826 mediated delivery of VEGF-C potently reduces chronic skin inflammation. *JCI Insight.*  
827 2018;3(23).
- 828 44. Skopelja-Gardner S, Tai J, Sun X, Tanaka L, Kuchenbecker JA, Snyder JM, et al. Acute skin  
829 exposure to ultraviolet light triggers neutrophil-mediated kidney inflammation. *Proc*  
830 *Natl Acad Sci U S A.* 2021;118(3).
- 831 45. Liu Y, Seto NL, Carmona-Rivera C, and Kaplan MJ. Accelerated model of lupus  
832 autoimmunity and vasculopathy driven by toll-like receptor 7/9 imbalance. *Lupus*  
833 *Science & Medicine.* 2018;5(1):e000259.
- 834 46. Lewis SM, Williams A, and Eisenbarth SC. Structure and function of the immune system  
835 in the spleen. *Sci Immunol.* 2019;4(33).
- 836 47. Vieira P, and Rajewsky K. The half-lives of serum immunoglobulins in adult mice. *Eur J*  
837 *Immunol.* 1988;18(2):313-6.
- 838 48. Hodgkinson LM, Wu TT, and Fiorentino DF. Dermatomyositis autoantibodies: how can  
839 we maximize utility? *Annals of translational medicine.* 2021;9(5):433.
- 840 49. Kajiya K, Sawane M, Huggenberger R, and Detmar M. Activation of the VEGFR-3 pathway  
841 by VEGF-C attenuates UVB-induced edema formation and skin inflammation by  
842 promoting lymphangiogenesis. *J Invest Dermatol.* 2009;129(5):1292-8.
- 843 50. Mohr E, Serre K, Manz RA, Cunningham AF, Khan M, Hardie DL, et al. Dendritic cells and  
844 monocyte/macrophages that create the IL-6/APRIL-rich lymph node microenvironments  
845 where plasmablasts mature. *J Immunol.* 2009;182(4):2113-23.

- 846 51. Smith MH, Gao VR, Periyakoil PK, Kochen A, DiCarlo EF, Goodman SM, et al. Drivers of  
847 heterogeneity in synovial fibroblasts in rheumatoid arthritis. *Nature Immunology*.  
848 2023;24(7):1200-10.
- 849 52. Wei K, Korsunsky I, Marshall JL, Gao A, Watts GFM, Major T, et al. Notch signalling drives  
850 synovial fibroblast identity and arthritis pathology. *Nature*. 2020;582(7811):259-64.
- 851 53. Tomei AA, Siegert S, Britschgi MR, Luther SA, and Swartz MA. Fluid flow regulates  
852 stromal cell organization and CCL21 expression in a tissue-engineered lymph node  
853 microenvironment. *J Immunol*. 2009;183(7):4273-83.
- 854 54. Horsnell HL, Tetley RJ, De Belly H, Makris S, Millward LJ, Benjamin AC, et al. Lymph node  
855 homeostasis and adaptation to immune challenge resolved by fibroblast network  
856 mechanics. *Nat Immunol*. 2022;23(8):1169-82.
- 857 55. Assen FP, Abe J, Hons M, Hauschild R, Shamipour S, Kaufmann WA, et al. Multitier  
858 mechanics control stromal adaptations in the swelling lymph node. *Nat Immunol*.  
859 2022;23(8):1246-55.
- 860 56. Howlader MJ, Rashighi M, Santambrogio L, and Lu TT. Lymphatic messengers: Non-  
861 antigen soluble mediators from diseased tissues to draining lymph nodes. *Curr Opin*  
862 *Immunol*. 2025;93:102536.
- 863 57. Perez-Shibayama C, Islander U, Lütge M, Cheng HW, Onder L, Ring SS, et al. Type I  
864 interferon signaling in fibroblastic reticular cells prevents exhaustive activation of  
865 antiviral CD8(+) T cells. *Sci Immunol*. 2020;5(51).
- 866 58. Platt AM, Rutkowski JM, Martel C, Kuan EL, Ivanov S, Swartz MA, et al. Normal dendritic  
867 cell mobilization to lymph nodes under conditions of severe lymphatic hypoplasia. *J*  
868 *Immunol*. 2013;190(9):4608-20.
- 869 59. Kumar V, Dasoveanu DC, Chyou S, Tzeng T-C, Rozo C, Liang Y, et al. A dendritic-cell-  
870 stromal axis maintains immune responses in lymph nodes. *Immunity*. 2015;42:719-30.
- 871 60. Loo CP, Nelson NA, Lane RS, Booth JL, Loprinzi Hardin SC, Thomas A, et al. Lymphatic  
872 Vessels Balance Viral Dissemination and Immune Activation following Cutaneous Viral  
873 Infection. *Cell Reports*. 2017;20(13):3176-87.
- 874 61. Billi AC, Ma F, Plazyo O, Gharaee-Kermani M, Wasikowski R, Hile GA, et al. Nonlesional  
875 lupus skin contributes to inflammatory education of myeloid cells and primes for  
876 cutaneous inflammation. *Science Translational Medicine*. 2022;14(642):eabn2263.
- 877 62. Der E, Suryawanshi H, Morozov P, Kustagi M, Goilav B, Ranabothu S, et al. Tubular cell  
878 and keratinocyte single-cell transcriptomics applied to lupus nephritis reveal type I IFN  
879 and fibrosis relevant pathways. *Nat Immunol*. 2019;20(7):915-27.
- 880 63. Psarras A, Alase A, Antanaviciute A, Carr IM, Md Yusof MY, Wittmann M, et al.  
881 Functionally impaired plasmacytoid dendritic cells and non-haematopoietic sources of  
882 type I interferon characterize human autoimmunity. *Nature Communications*.  
883 2020;11(1):6149.
- 884 64. Li TM, Zyulina V, Seltzer ES, Dacic M, Chinenov Y, Daamen AR, et al. The interferon-rich  
885 skin environment regulates Langerhans cell ADAM17 to promote photosensitivity in  
886 lupus. *eLife*. 2024;13:e85914.
- 887 65. Skopelja-Gardner S, An J, Tai J, Tanaka L, Sun X, Hermanson P, et al. The early local and  
888 systemic Type I interferon responses to ultraviolet B light exposure are cGAS dependent.  
889 *Sci Rep*. 2020;10(1):7908.

- 890 66. Clement CC, D'Alessandro A, Thangaswamy S, Chalmers S, Furtado R, Spada S, et al. 3-  
891 hydroxy-L-kynurenamine is an immunomodulatory biogenic amine. *Nat Commun.*  
892 2021;12(1):4447.
- 893 67. Russo E, Teixeira A, Vaahtomeri K, Willrodt AH, Bloch JS, Nitschke M, et al.  
894 Intralymphatic CCL21 Promotes Tissue Egress of Dendritic Cells through Afferent  
895 Lymphatic Vessels. *Cell Rep.* 2016;14(7):1723-34.
- 896 68. Saxena V, Piao W, Li L, Paluskievicz C, Xiong Y, Simon T, et al. Treg tissue stability  
897 depends on lymphotoxin beta-receptor- and adenosine-receptor-driven lymphatic  
898 endothelial cell responses. *Cell Rep.* 2022;39(3):110727.
- 899 69. Lu B, Rutledge BJ, Gu L, Fiorillo J, Lukacs NW, Kunkel SL, et al. Abnormalities in monocyte  
900 recruitment and cytokine expression in monocyte chemoattractant protein 1-deficient  
901 mice. *J Exp Med.* 1998;187(4):601-8.
- 902 70. Shi C, Jia T, Mendez-Ferrer S, Hohl TM, Serbina NV, Lipuma L, et al. Bone marrow  
903 mesenchymal stem and progenitor cells induce monocyte emigration in response to  
904 circulating toll-like receptor ligands. *Immunity.* 2011;34(4):590-601.
- 905 71. Hohl TM, Rivera A, Lipuma L, Gallegos A, Shi C, Mack M, et al. Inflammatory monocytes  
906 facilitate adaptive CD4 T cell responses during respiratory fungal infection. *Cell Host*  
907 *Microbe.* 2009;6(5):470-81.
- 908 72. Escobedo N, Proulx ST, Karaman S, Dillard ME, Johnson N, Detmar M, et al. Restoration  
909 of lymphatic function rescues obesity in Prox1-haploinsufficient mice. *JCI Insight.*  
910 2016;1(2).
- 911 73. Chia JJ, Zhu T, Chyou S, Dasoveanu DC, Carballo C, Tian S, et al. Dendritic cells maintain  
912 dermal adipose-derived stromal cells in skin fibrosis. *J Clin Invest.* 2016;126(11):4331-45.
- 913 74. Chyou S, Benahmed F, Chen J, Kumar V, Tian S, Lipp M, et al. Coordinated regulation of  
914 lymph node vascular-stromal growth first by CD11c+ cells and then by T and B cells. *J*  
915 *Immunol.* 2011;187(11):5558-67.

916

917



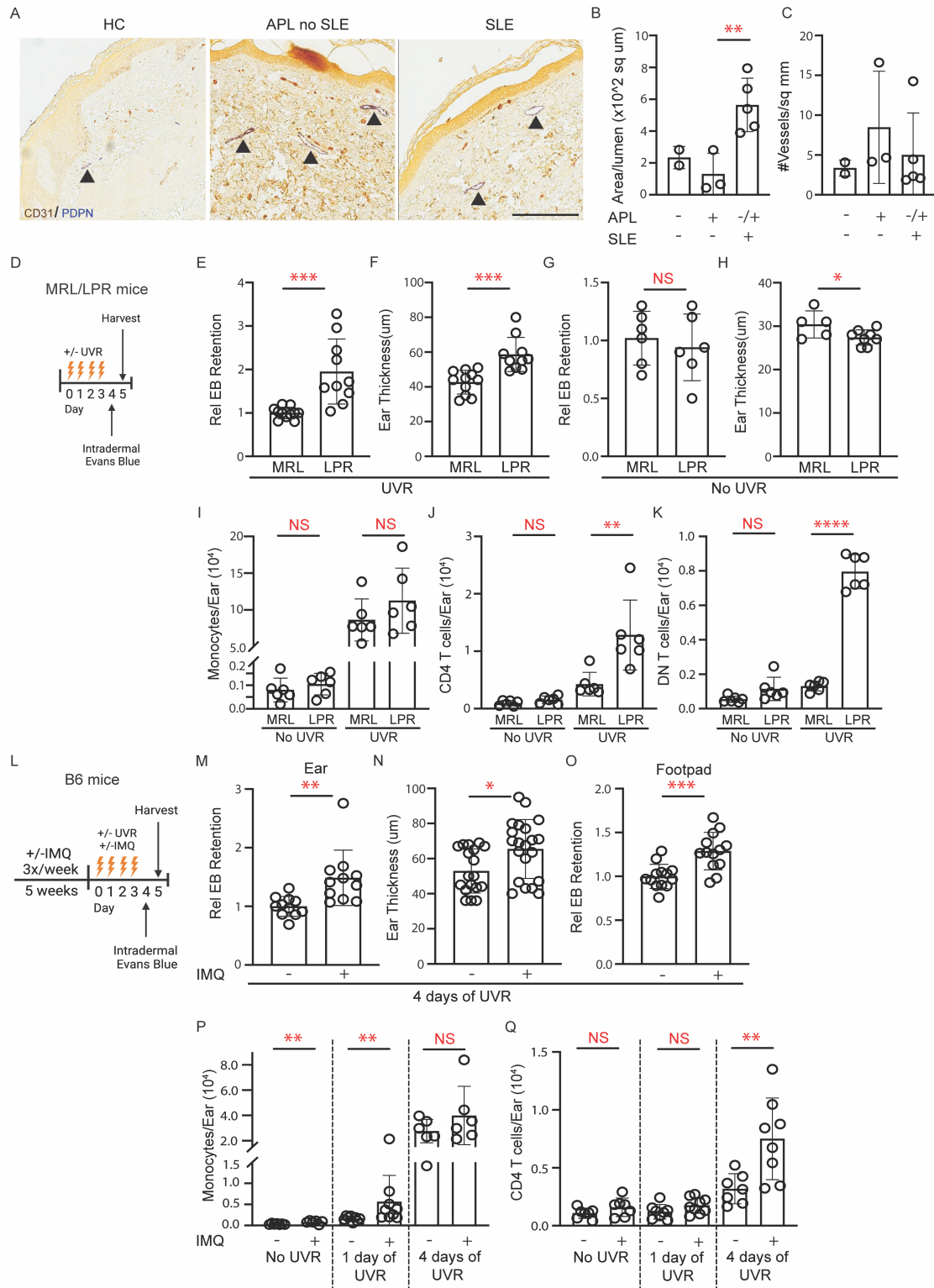


**Figure 1. Patients with SLE and murine SLE models show evidence of cutaneous lymphatic dysfunction**

(A-C) Punch biopsies of forearm skin from healthy control (HC), positive antiphospholipid antibodies (APL) without SLE, and SLE subjects with or without APL were stained for CD31+PDPN+ lymphatic vessels. (A) Representative photomicrographs. Arrowheads point to lymphatic vessels. (B) Lumenal area per vessel. Each symbol is an individual subject. (C) Number of lymphatic vessels per tissue area. (D-H) LPR mice and MRL controls were treated with ultraviolet radiation (UVR) for 4 consecutive days, injected in ear pinna with Evans blue dye (EB) 1 day after final UVR dose, and ear harvested to assess EB content 1 day later, as in (D). (E) EB retention and (F) ear swelling was quantified after UVR or (G,H) with no UVR. (I-K) Ears were examined by flow cytometry at 24 hours after final dose of UVR. (I) Monocyte, (J) TCR $\alpha\beta$  CD4+ T cell, and (K) TCR $\alpha\beta$  CD3+ CD4-CD8- “double negative” (DN) T cell numbers. (L-O) B6 mice received IMQ on the right ear and exposed to UVR, and EB retention after intradermal injection of left ear or footpad was compared to responses in vehicle-treated control mice, as in (L). (M) EB retention in ear. (N) Ear swelling. (O) EB retention in footpad. (P-Q) Left ear was collected 24 hours after 1 or 4 doses of UVR. (P) Monocyte and (Q) TCR $\alpha\beta$  CD4 T cell numbers. Each symbol represents one mouse; n = 2 to 21 per condition; data are from 2 (I, J, K), 3 (M, O), 4 (G, H), 6 (E, F), 10 (N), and 11 (P, Q) independent experiments. Normality was assessed using the Shapiro-Wilk test. If normal, unpaired t test was used. If data were not normal, Mann-Whitney U test was used. \*\*\*P<0.001, \*\*P<0.01, \*P<0.05, NS=not significant. Error bars represent SD.

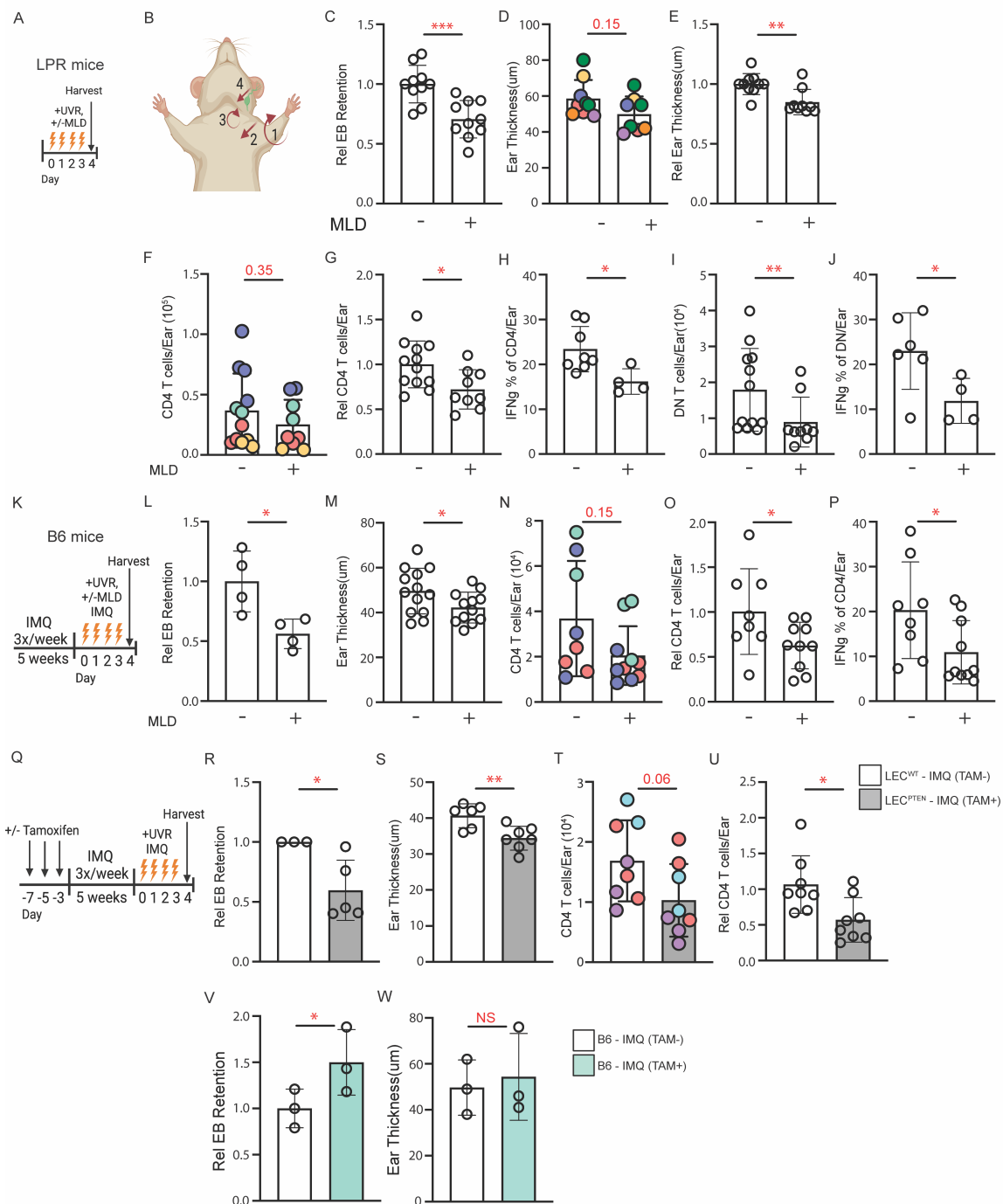


**Figure 2. Improving lymphatic flow reduces cutaneous photosensitive responses in SLE models**

(A-J) LPR mice and (K-P) B6-IMQ mice were treated with UVR and manual lymphatic drainage (MLD) targeting the left ear or were control handled. Left ear was then

examined. (A, K) Experimental design. (B) Illustration of MLD technique. Please see  
Methods for details. (C, L) EB retention and (D, E, M) ear thickness, absolute (D,M) or  
normalized (E). (F, N) TCR $\alpha\beta$  CD4 T cell numbers, (G,O) normalized to controls. (H, P)  
Percentage of CD4 T cells that express IFN $\gamma$ . (I) DN T cell numbers and (J) percentage  
that express IFN $\gamma$ . (Q-U) Flt4Cre<sup>ERT2</sup> PTEN<sup>fl/fl</sup> mice treated with tamoxifen (LEC<sup>PTEN</sup>) or  
without (LEC<sup>WT</sup>) were treated with IMQ on right ear and UVR before left ear skin  
assessment, as in (Q). (R) EB retention, (S) skin thickness, (T) TCR $\alpha\beta$  CD4 T cell  
numbers, and (U) IFN $\gamma$ + percentage. (V, W) Non-transgenic B6 mice were treated as  
described in (Q). (V) EB retention and (W) ear thickness. Each symbol represents one  
mouse; n= 3 to 13 per condition; data are from 2 (H, J, L, V, W), 3 (N, O, P, R, T, U), 4 (F,  
G, I, S), 6 (C), 7 (D, E), and 9 (M) independent experiments. Normality was assessed  
using the Shapiro-Wilk test. If normal, unpaired t test was used. If data were not normal,  
Mann-Whitney U test was used. \*\*\*P<0.001, \*\*P<0.01, \*P<0.05, NS=not significant.  
Error bars represent SD.

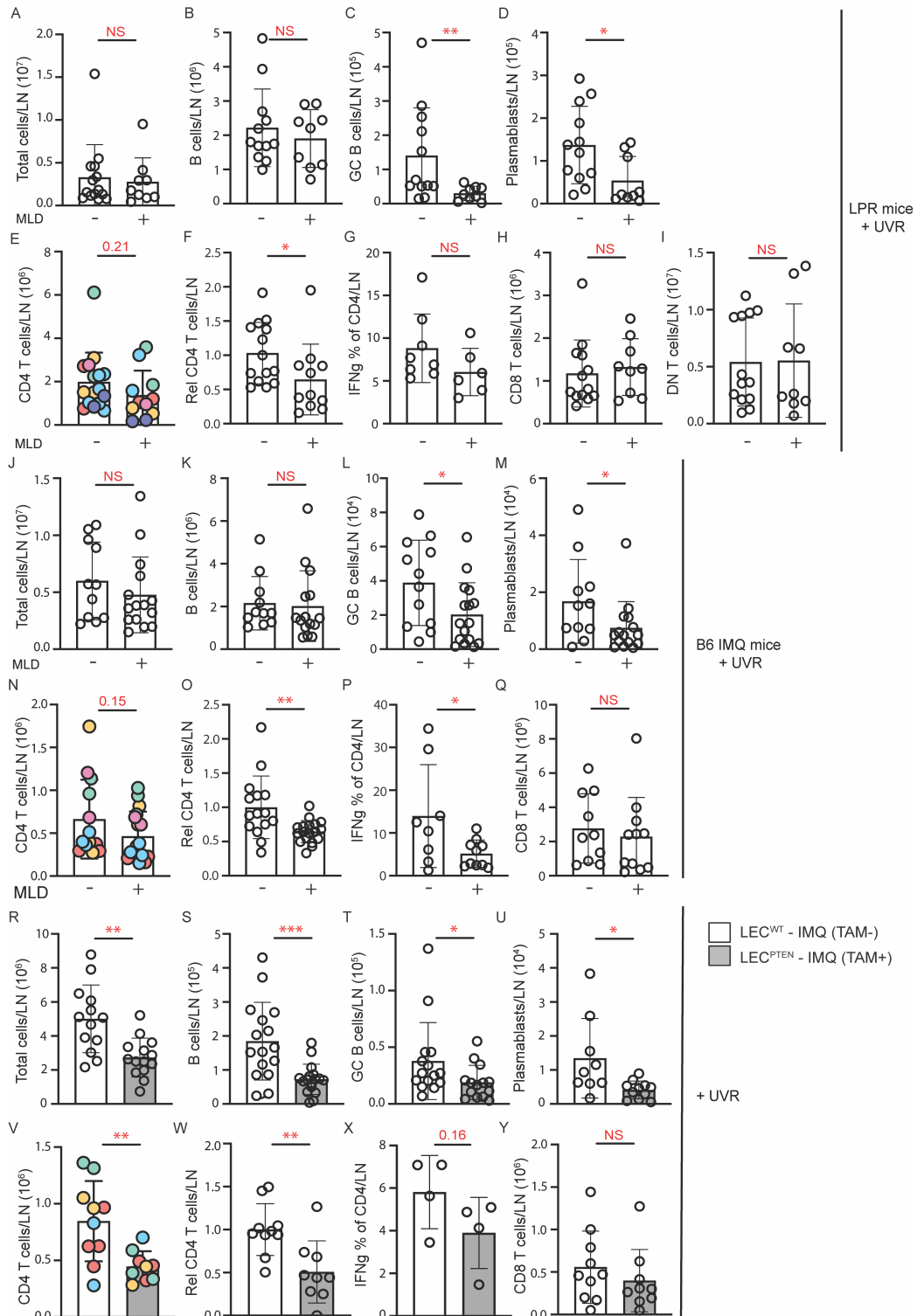


**Figure 3. Improving lymphatic flow reduces draining lymph node B and T cell responses in SLE models**

(A-Q) Left auricular lymph nodes of (A-I) LPR, (J-Q) B6-IMQ, and (R-X) LEC<sup>PTEN</sup>-IMQ and LEC<sup>WT</sup>-IMQ mice that were treated as in Figure 2A, K, and Q were examined. (A, J, R) Lymph node cellularity. (B, K, S) B cell, (C, L, T) germinal center B cell, (D, M, U) plasmablast, and (E, N, V) TCR $\alpha\beta$  CD4 T cell numbers. (F, O, W) CD4 T cell numbers normalized to control. (G, P, X) Percentage of CD4 T cells that express IFN $\gamma$ . (H, Q, Y) CD8 and (I) DN T cell numbers. Each symbol represents one mouse; n= 4 to 17 per condition; data are from 2 (X), 3 (G, P, Q), 4 (A-C, H-K, M, V, W, Y), 5 (D, N, O), 6 (E, F, L, R, U), and 8 (S, T) independent experiments. Normality was assessed using the Shapiro-Wilk test. If normal, unpaired t test was used. If data were not normal, Mann-Whitney U test was used. \*\*\*P<0.001, \*\*P<0.01, \*P<0.05, NS=not significant. Error bars represent SD.

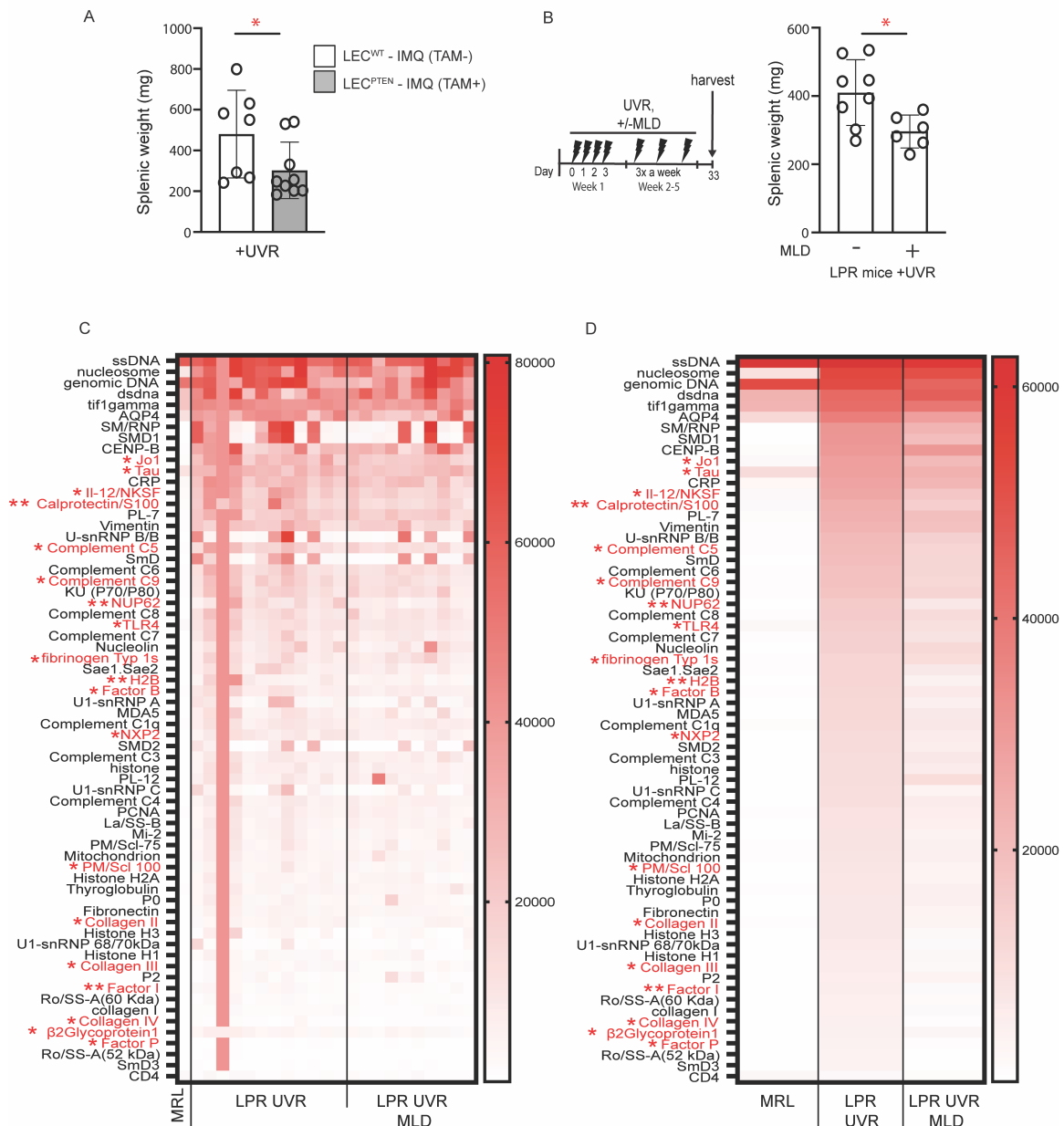


**Figure 4. Improving lymphatic flow long term reduces systemic disease activity**

(A) Splenic weight of LEC<sup>PTEN</sup>-IMQ and LEC<sup>WT</sup>-IMQ mice treated with UVR for 4 days.

(B) Splenic weight of LPR mice treated with UVR and MLD concurrently or control

handled for 5 weeks. (C,D) Heatmap of normalized signal intensity (NSI) from

autoantigen microarray panel for IgG of MRL mice, LPR mice treated with UVR, and

LPR mice treated with both UVR and MLD for 4-5 weeks. (C) Each column represents

one mouse and autoantibodies with significant differences between LPR UV and LPR UV+MLD are labelled in red. (D) Each column represents average NSI of all mice serum samples. Each symbol represents one mouse; n= 1 to 12 per condition; data are from 1 (B), 2 (C, D), and 6 (A) independent experiments. Normality was assessed using the Shapiro-Wilk test. If normal, unpaired t test was used. If data were not normal, Mann-Whitney U test was used. \*\*\*P<0.001, \*\*P<0.01, \*P<0.05, NS=not significant. Error bars represent SD.



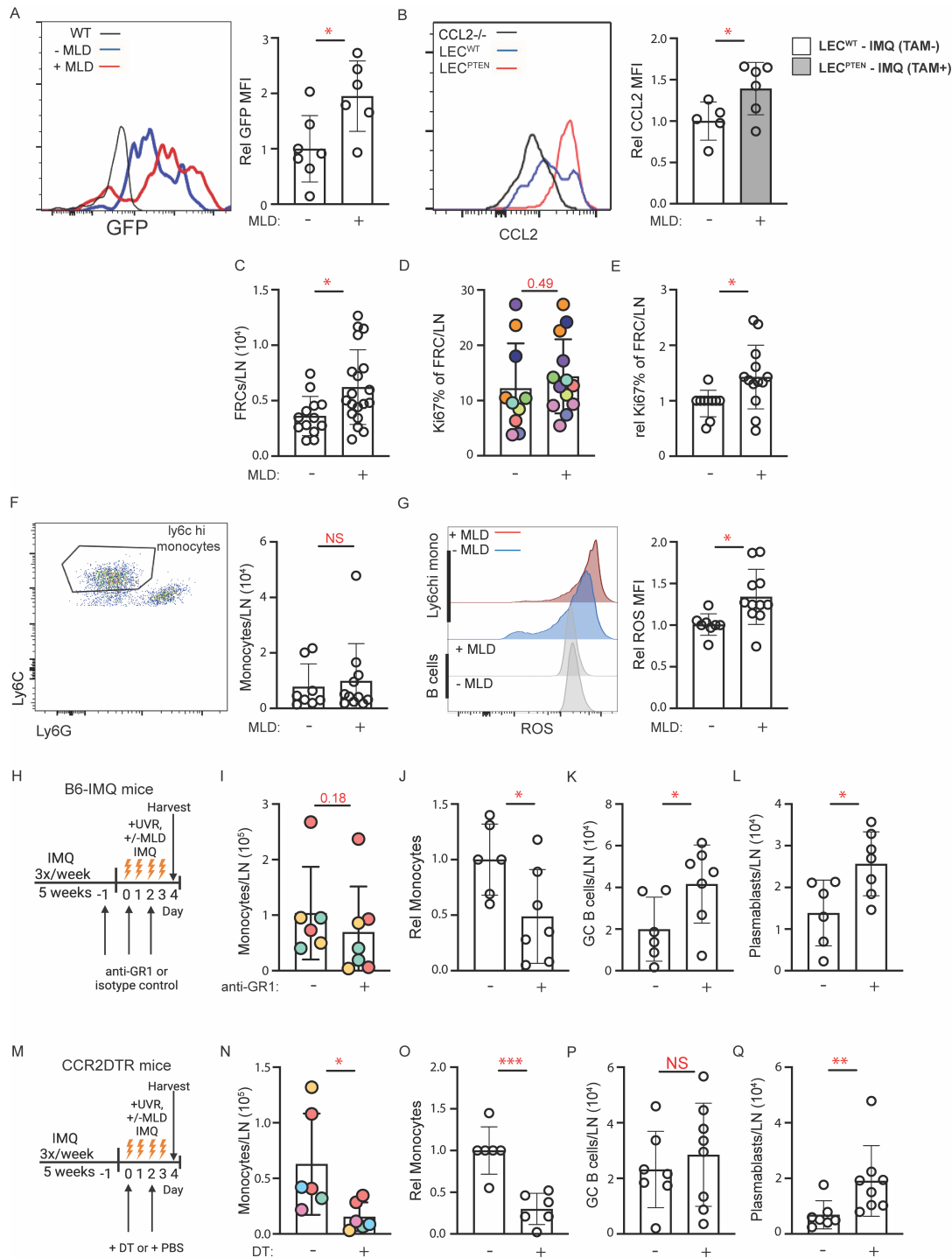


**Figure 5. Improving lymphatic flow increases lymph node FRC proliferation, FRC CCL2, monocyte ROS generation, and limits plasmablast numbers in a monocyte-dependent manner**

(A-Q) Left auricular lymph nodes of indicated mice exposed to 4 days of UVR were examined. (A) FRC expression of GFP in CCL2-GFP reporter mice treated with IMQ that received MLD or control handling with UVR. (B) CCL2 expression by FRCs in LEC<sup>PTEN</sup>-IMQ and LEC<sup>WT</sup>-IMQ mice. (A, B) Representative histogram (left) and graph (right). MFI=geometric mean fluorescence intensity. (C-G) B6-IMQ mice received 4 days of +/-MLD with UVR. (C) FRC numbers. (D) Percentage of FRCs that express ki67, (E) normalized to control handled mice. (F) Ly6C<sup>hi</sup> monocyte numbers, flow cytometry gating (left) and numbers (right). (G) Monocyte ROS measured using CM-H2DCFDA, representative histograms (left) and relative MFI of CM-H2DCFDA (right). (H-L) B6-IMQ mice were treated with anti-Gr-1 or isotype control at days -1, 0, and +2 of UVR and MLD treatments as shown in (H). (I) Monocyte numbers and (J) normalized to isotype control. (K) Germinal center B cell and (L) plasmablast numbers. (M-Q) CCR2-DTR mice were treated with DT at days 0 and 2 of UVR and MLD treatments as shown in (M). (N) Monocyte numbers and (O) normalized to control. (P) Germinal center B cell and (Q) plasmablast numbers. Each symbol represents one mouse; n= 6 to 19 per condition; data are from 2 (B), 3 (A, I-L), 5 (N, O), 6 (D-G, P, Q), and 7 (C) independent experiments. Normality was assessed using the Shapiro-Wilk test. If normal, unpaired t test was used. If data were not normal, Mann-Whitney U test was used. \*\*\*P<0.001, \*\*P<0.01, \*P<0.05, NS=not significant. Error bars represent SD.